Numerical study of sediment and ^{137}Cs discharge out of reservoirs during various scale rainfall events

Hiroshi Kurikami[1,*], Hironori Funaki[2], Alex Malins[3], Akihiro Kitamura[4] and Yasuo Onishi[5]

[1]Japan Atomic Energy Agency (JAEA), Sector of Fukushima Research and Development, 10-2 Fukasaku, Miharu-machi, Tamura-gun, Fukushima 963-7700, Japan, kurikami.hiroshi@jaea.go.jp, Tel: +81-247-61-2910

[2]Japan Atomic Energy Agency (JAEA), Sector of Fukushima Research and Development, 10-2 Fukasaku, Miharu-machi, Tamura-gun, Fukushima 963-7700, Japan, funaki.hironori@jaea.go.jp

[3]Japan Atomic Energy Agency (JAEA), Center for Computational Science & e-Systems, University of Tokyo Kashiwanoha Campus Satellite, 178-4-4 Wakashiba, Kashiwa, Chiba 277-0871, Japan, malins.alex@jaea.go.jp

[4]Japan Atomic Energy Agency (JAEA), Sector of Fukushima Research and Development, 10-2 Fukasaku, Miharu-machi, Tamura-gun, Fukushima 963-7700, Japan, kitamura.akihiro@jaea.go.jp

[5]Yasuo Onishi Consulting, LLC, Richland, WA 99354, U.S.A. and formerly Pacific Northwest National Laboratory (PNNL), Fluid & Computational Engineering, P.O.Box 999, Richland, WA 99352, U.S.A., yasuo.onishi@yahoo.com

*Corresponding author

Highlights

- Systematic analysis of sediment and ^{137}Cs discharge from generic models of reservoirs.
- Parameters employed (flood intensity, reservoir volume and K_d) are similar to those occurring in Fukushima.
- Simulations determine the effect of these parameters on radiocesium discharge.
- ^{137}Cs mainly discharges in silt-sorbed form in larg floods, while clay-sorbed and dissolved forms dominate in small events.
- Results can be used to estimate ^{137}Cs discharges from reservoirs in arbitrary flood events.

Abstract

Contamination of reservoirs with radiocesium is one of the main concerns in Fukushima Prefecture, Japan. We performed simulations using the three-dimensional finite volume code FLESCOT to understand sediment and radiocesium transport in generic models of reservoirs with parameters similar to those in Fukushima Prefecture. The simulations model turbulent water flows, transport of sediments with different grain sizes, and radiocesium migration both in dissolved and particulate forms. To demonstrate the validity of the modeling approach for the Fukushima environment, we performed a test simulation of the Ogaki Dam reservoir over Typhoon Man-yi in September 2013 and compared the results with field measurements. We simulated a set of generic model reservoirs systematically varying features such as flood intensity, reservoir volume and the radiocesium distribution coefficient. The results ascertain how these features affect the amount of sediment or ^{137}Cs discharge downstream from the reservoirs, and the forms in which ^{137}Cs is discharged. Silt carries the majority of the radiocesium in the larger flood events, while the clay-sorbed followed by dissolved forms are dominant in smaller events. The results can be used to derive indicative values of discharges from Fukushima reservoirs under arbitrary flood events. For example the generic model simulations indicate that about 30% of radiocesium that entered the Ogaki Dam reservoir over the flood in September 2015 caused by Typhoon Etau discharged downstream. Continued monitoring and numerical predictions are necessary to quantify future radiocesium migration in Fukushima Prefecture and evaluate possible countermeasures since reservoirs can be a sink of radiocesium.

1. Introduction

Although most of the radiocesium within Fukushima Prefecture remains adsorbed to

soils on the ground surface, accumulations can be found within reservoirs across the region. Identifying practical countermeasures against radiocesium migration within the Prefecture is an important issue, particularly as there are ~3,700 reservoirs within the region used for irrigation, surface water management and drinking water supply.

For example, discussions are ongoing at the Prefectural level for implementing countermeasures against contamination in the Ogaki Dam reservoir, which is located in one of the highest radioactive fallout regions of Fukushima. This is in prospect of residents returning and restarting agriculture downstream of the Ogaki Dam. There is particular concern about outflow of contaminants from Fukushima's reservoirs during typhoon floods and the long term contamination of the reservoir and river ecosystems with radiocesium. It is essential to understand the behavior of radiocesium in reservoirs to evaluate potential countermeasure options.

Various investigators have studied aquatic systems affected by fallout from atmospheric nuclear weapons testing and the Chernobyl nuclear accident. Based on field investigations and modeling studies, Smith et al. (2002) classified lakes as either closed or open depending on water residence times; closed lakes have long water residence times, while open lakes have a more rapid turnover of the reservoir water. In closed lakes, resuspension and remobilization from the bed sediments dominate long term migration of radioactivity in the lake (Smith et al., 2002). In the vicinity of Chernobyl, closed lakes tended to have higher activity concentrations in the water and aquatic biota than typical open lakes and rivers (Bulgakov et al., 2002; IAEA, 2006). In open lakes, the input of radioactivity is dominated by inflow from the upstream catchment (Smith et al., 2002). Spezzano et al. (1993) reported that lakes in catchments containing soils poor in clay minerals were likely to receive significant radiocesium input from the catchment, resulting in a high concentration of radiocesium in such lakes.

After the Fukushima accident, there have been many reports of open lakes containing

high accumulations of radiocesium (e.g. Ochiai et al., 2013; Chartin et al., 2013; Mouri et al., 2014). Evrard et al. (2013, 2014) found that dam releases are a major factor controlling dispersion of contaminated sediment in Fukushima Prefecture. In our previous numerical studies, we identified that reservoirs play an important role in delaying and buffering the movement of radiocesium in heavy rainfall events (Kurikami et al., 2014; Yamada et al, 2015). Buffering of radiocesium in a reservoir depends strongly on the reservoir water level and migration behavior of different sediment grades. In a review of the literature related to the accident at the Fukushima Dai-ichi Nuclear Power Plant, Evrard et al. (2015) concluded that the majority of radiocesium is transported from hillslopes to the ocean in the particulate fraction, attached to fine sediments during major runoff events. The importance of the particulate fraction is higher than seen in Ukraine after the Chernobyl accident, explained by the relatively high distribution coefficient of radiocesium to Fukushima soils.

This paper describes simulations using the FLESCOT code to understand the discharge of radiocesium during flood events. An application of FLECOT is presented for the Ogaki Dam reservoir over Typhoon Man-yi in 2013. The results of this simulation were validated against results from field investigations. A set of simulations of generic models for reservoirs are reported, where the parameters affecting radiocesium discharge were varied systematically. The results determine the effect of flood intensity and duration, reservoir volume and the radiocesium distribution coefficient on radiocesium discharges from the reservoirs. Future discharges from reservoirs in Fukushima Prefecture can be gauged using the results.

2. Material and methods

2.1 Model Description

The FLESCOT (Flow, Energy, Salinity, Sediment Contaminant Transport) code used in

this study was developed by the Pacific Northwest National Laboratory (Onishi et al., 1993). FLESCOT is a 3D finite-volume code that calculates distributions of flow, turbulent kinetic energy and its dissipation, water temperature, salinity, sediment concentrations of suspended sand, silt and clay, dissolved and particulate radionuclide concentrations. It also simulates changes in fractions of sand, silt and clay within bottom sediments and radionuclide concentrations adsorbed by bottom sediments. The code has been applied to various contaminants, including radionuclides, heavy metals and toxic organic chemicals. An example case study is ^{137}Cs redistribution within the Hudson River Estuary (Onishi and Trent, 1985; Onishi et al., 1987; Onishi and Trent, 1992; Onishi et al., 1993).

The equations governing sediment transport that FLESCOT solves are

$$\frac{\partial c_i}{\partial t}+\frac{\partial}{\partial x}(uc_i)+\frac{\partial}{\partial y}(wc_i)+\frac{\partial}{\partial z}[(v-v_{si})c_i] = \frac{\partial}{\partial x}\left(\varepsilon_x\frac{\partial c_i}{\partial x}\right)+\frac{\partial}{\partial y}\left(\varepsilon_y\frac{\partial c_i}{\partial y}\right)+\frac{\partial}{\partial z}\left(\varepsilon_z\frac{\partial c_i}{\partial z}\right)+\left(\frac{s_{ri}}{h}-\frac{s_{di}}{h}\right)+q_{ci} \quad (1)$$

where c_i (kg/m^3) is the i^{th} sediment concentration per unit volume, t (s) is time, u, w and v (m/s) are flow velocities in x-, y- and z-directions, v_{si} (m/s) is the settling velocity of the i^{th} sediment, ε_x, ε_y and ε_z (m^2/s) are dispersion coefficients in x-, y- and z-directions, s_{ri} (kg/m^2/s) is the i^{th} sediment erosion rate per unit surface area, s_{di} (kg/m^2/s) is the i^{th} sediment deposition rate per unit surface area, h (m) is the flow depth, and q_{ci} (kg/m^3/s) is the source of i^{th} sediment.

The transport equation of dissolved radioactive species is

$$\frac{\partial g}{\partial t}+\frac{\partial}{\partial x}(ug)+\frac{\partial}{\partial y}(wg)+\frac{\partial}{\partial z}(vg) = \frac{\partial}{\partial x}\left(\varepsilon_x\frac{\partial g}{\partial x}\right)+\frac{\partial}{\partial y}\left(\varepsilon_y\frac{\partial g}{\partial y}\right)+\frac{\partial}{\partial z}\left(\varepsilon_z\frac{\partial g}{\partial z}\right)-\lambda g - \sum_{i=1}^{3}K_i(c_iK_{di}g-g_i)-\frac{1}{h}\sum_{i=1}^{3}\gamma_i(1-n)d_iK_{bi}(K_{di}g-g_{bi}) \quad (2)$$

where g (Bq/m^3) is the dissolved radiocesium concentration per unit volume, λ (s^{-1}) is the radionuclide decay constant, K_i and K_{bi} (s^{-1}) are transfer rates of radiocesium between the i^{th}

suspended sediment and bed sediment by adsorption/desorption, K_{di} (m^3/kg) is the distribution coefficient between dissolved cesium and particulate cesium associated with the i^{th} sediment for adsorption/desorption, g_i (Bq/m^3) is the particulate cesium concentration per unit volume associated with the i^{th} sediment, γ_i is the specific weight of the i^{th} sediment, n (m^3/m^3) is the porosity of bed sediment, d_i (m) is the particle diameter of the i^{th} sediment, and g_{bi} (Bq/kg) is the particulate cesium concentration per unit weight of the i^{th} sediment in the bed.

The transport equations of particulate radioactive species is

$$\frac{\partial g_i}{\partial t}+\frac{\partial}{\partial x}(ug_i)+\frac{\partial}{\partial y}(wg_i)+\frac{\partial}{\partial z}\left[(v-v_{si})g_i\right]=\frac{\partial}{\partial x}\left(\varepsilon_x\frac{\partial g_i}{\partial x}\right)+\frac{\partial}{\partial y}\left(\varepsilon_y\frac{\partial g_i}{\partial y}\right)+\frac{\partial}{\partial z}\left(\varepsilon_z\frac{\partial g_i}{\partial z}\right)$$
$$-\lambda g_i-\frac{s_{di}}{h}g_i+K_i\left(c_iK_{di}g-g_i\right)+\frac{g_{bi}s_{ri}}{h}+q_i \qquad (3)$$

where q_i (Bq/m^3/s) is the source of particulate cesium associated with the i^{th} sediment.

2.2 Simulation of the Ogaki Dam reservoir

To validate FLESCOT in the Fukushima environment, we applied the code to the Ogaki Dam reservoir. The reservoir is located in the middle reaches of the Ukedo River (Fig. 1), approximately 17 km north-west from the Fukushima Dai-ichi Nuclear Power Plant. The reservoir supplied irrigation water to paddy fields in the downstream Ukedo River area prior to March 2011. After the radioactive fallout, the area surrounding the reservoir was evacuated and the dam operation suspended. The water level was artificially lowered to protect the dam against further earthquakes and to allow structural checks to take place.

The upper part of the Ukedo catchment is one of the most contaminated areas of Fukushima Prefecture. It is designated as an area where residents are not expected to be able to return to (Ministry of Economy, Trade and Industry, 2013). The coastal part of the Ukedo catchment suffered lower fallout levels, and the radiation levels are now sufficiently low in

many areas to allow residents to return. The question of how to resume economic activities such as agriculture, requiring reutilization of the dam, is an important social issue.

Japan Atomic Energy Agency (JAEA) and the Japanese Ministry of Agriculture, Forestry and Fisheries (MAFF) have performed a series of field studies on the Ogaki Dam reservoir. Japan Atomic Energy Agency monitored the vertical profiles of the water flow velocity, turbidity and temperature at two monitoring points (St. 1 and St. 2) in the reservoir. The Japanese Ministry of Agriculture, Forestry and Fisheries monitored river discharge rates, the concentration of suspended sediment and radiocesium in the river water at three monitoring stations (two above the reservoir and one at the outlet). The monitoring points are shown in Fig. 1.

The majority of sediment and radiocesium migration in Fukushima Prefecture occurs over typhoon floods (e.g., Yamashiki et al., 2014; Ueda et al., 2013; Nagao et al., 2013). We simulated the behavior of sediment and radiocesium in the reservoir during a large flood by Typhoon Man-yi in September 2013 due to the wide availability of monitoring data for water, sediment and radiocesium flows for this event. Figure 2 shows the topography of the Ogaki Dam reservoir bed. When the reservoir water height is set at 140 m above sea level, the average water depth in the reservoir is 9.1 m. The FLESCOT model discretized the area into cells with average size 10 m (NS) x 10 m (EW) x 2 m (vertical), giving a total of 12,696 computational cells.

As boundary conditions for our simulations, we employed monitored values (MAFF, 2014; MAFF, private communication, January 28, 2014) of the river flow rate, the concentration of suspended sediment and the concentration of ^{137}Cs taken at monitoring stations (Hirusone and Yaguno in Fig. 1) on the upstream tributaries of the reservoir. These data are shown in Figs. 3, 4 and 5, respectively. Data were unavailable for the concentrations of suspended sediment and ^{137}Cs for the period from September 16, 6:00 to September 17,

12:00. A second flow peak occurred within this period. The suspended sediment concentrations for this period were estimated by multiplying the flow rate within the period (data in Fig. 3) by the average suspended sediment to flow rate ratio (data in Fig. 4) at equal flow rates during other periods (data in Fig. 4). Likewise the ^{137}Cs concentrations between September 16, 6:00 and September 17, 12:00 were estimated using the ^{137}Cs concentrations at equal flow rates at times outside this period (Fig. 5).

The fractions of sand, silt and clay as the inflow boundary condition were set based on measurements by MAFF. While the bulk concentrations of radiocesium (containing dissolved and particulate cesium) were measured, the dissolved and particulate cesium concentrations were not measured separately. Thus, we estimated the concentrations of particulate and dissolved radiocesium from the total based on the distribution coefficients of sand, silt and clay measured in field samples (JAEA, 2013a, 2013b). The parameters used in the simulation are shown in Table 1. They are the same as those used in a previous study with a 1D simulation code (Kurikami et al, 2014), with the exception of dispersion coefficients that depend on the spatial dimension. The dispersion coefficients were estimated using the following International Atomic Energy Agency (IAEA) equation (IAEA, 2001)

$$\varepsilon_x = \varepsilon_y = \frac{uB^2}{3h} \tag{4}$$

$$\varepsilon_z = 0.0067uh \tag{5}$$

where B (m) is the width of the river/reservoir.

As initial conditions for within the reservoir, 0.5 mg/L of suspended sediment and 0.5 Bq/L of dissolved ^{137}Cs were applied based on our field data. The initial vertical temperature distribution shown in Fig. S1 in the supplementary material was assigned based

on JAEA's field investigations in September 2014, i.e. the same season but the following year from the September 2013 flood.

2.3 Systematic analysis of generic model reservoirs

There are about 3,700 reservoirs in Fukushima Prefecture, used for surface water management, irrigation and drinking water supply. The Japan Dam Foundation (2015) publishes various data on reservoirs in Japan. The reservoirs in Fukushima Prefecture have capacity varying between $3x10^4$ and $5x10^8$ m^3. We performed an analysis of how different scales of flood event (water inflow intensity and duration) affect the discharge rates of sediment and radiocesium downstream from reservoirs with capacities typical of those in Fukushima Prefecture. Figure 6 shows the model geometry, where the reservoir volume could be varied by adjusting the parameter a. Four reservoir volumes were considered: $V=10^5$ m^3 (width a=46.4 m), $V=10^6$ m^3 (a=100 m), $V=10^7$ m^3 (a=215.4 m) and $V=10^8$ m^3 (a=464.2 m), covering the typical range of volumes of reservoirs in Fukushima Prefecture.

Two types of rainfall events were applied: a shorter event and a longer event. The high flow period, T, of the shorter event was $1x10^4$ s (about 2.8 h), and for the longer event was $1x10^5$ s (about 28 h). Figure 7 shows the river inflow rate applied at the inlet boundary over the course of the model flood. Six cases of the river inflow rate during the high flow period, Q, were simulated for each volume reservoir, giving a total of 48 simulations. In each case Q was fixed such that QT/V was 0.3, 1.0, 2.0, 3.0, 5.0 or 7.0. QT/V represents the ratio of total inflow during the high flow period (m^3) to the reservoir volume (m^3), and therefore corresponds to the relative intensity of the flood event.

The inflow ratio of sand, silt and clay by mass concentration was assigned as 2:7:1, based on monitoring data for the Ogaki Dam reservoir. The dispersion coefficient was

195 calculated by using equations (4) and (5). The other parameters were the same as those for the
196 Ogaki Dam reservoir simulation. The water within the reservoir and the bed contained zero
197 sediment and radiocesium in the initial condition.

198 A second set of simulations focused on the distribution coefficient. Radiocesium
199 distribution coefficients of the soils in and around Fukushima vary from 1.2×10^{2} to
200 5.0×10^{3} m^3/kg, which are an order of magnitude greater than those reported by the IAEA after
201 the Chernobyl accident (2.9×10^{1} m^3/kg) (Evrard et al. 2015). In laboratory batch tests the
202 cesium distribution coefficient can vary between 1.0×10^{-2} and 6.7×10^{1} m^3/kg depending on
203 cation exchange capacity, clay content and concentrations of mica-like minerals (US
204 Environmental Protection Agency 1999).

205 We simulated five cases with QT/V=3.0, V=10^6 m^3 and the 28 h flood varying the
206 distribution coefficients K_{di} from 4×10^{-2} to 4×10^{2} m^3/kg. The simulations maintained the mass
207 ratio for sand, silt and clay as 2:7:1 at the inlet. The ratio of the distribution coefficients was
208 3:50:50 following the Ogaki simulation (Table 1). We scaled the distribution coefficients
209 according to this ratio for the sensitivity analysis.

210

211 3. Results and discussion

212 3.1 Simulation of the Ogaki Dam reservoir

213

214 To validate the FLESCOT code for simulating Fukushima reservoirs, we simulated the
215 concentrations of suspended sediment and ^{137}Cs at the outlet (monitoring station Exit marked
216 on Fig. 1) of the Ogaki Dam reservoir during a large typhoon in September 2013. Figs. 8 and
217 9 show comparisons of the simulation results and measurements of sediment and ^{137}Cs
218 outflow from the reservoir, respectively. The simulation results were in good agreement with
219 the measurements on the total concentrations of both suspended sediment and ^{137}Cs. However,

after the first peak of the flood (18:00 on September 15, 2013), the simulation predicted that the main sediment in the outflow is clay. This result is conflicting with the measurements, which found silt as the majority component.

We traced this discrepancy to the fact that the measurement counted flocculated matter as silt particles. Figure 10 shows microscope images of water samples taken from the inlet and the outlet of the reservoir during a flood event in October 2014. Suspended matters is visible in all the images. A large fraction of the clay particles are flocculated in the outlet samples (Fig. 10(b) and (c)). These flocculates were designated as silt by the measurement protocol, which classified the sediments based on size only. Therefore we explain the discrepancy by misclassification of the sediment grades in the measurement samples.

The settling velocity of flocculated matter is slower than that of other similarly sized sediments (e.g., Nishimura et al., 2009). Flocculated clays are therefore more likely to be transported across the reservoir and discharged downstream than silt particles. We also found that the suspended sediment in the outlet samples contained 10-30% organic matter, which acts to bind clay particles (Fig. 10(c)). Although organic matter has a low capacity to absorb cesium, it makes a significant contribution to the discharge of cesium from the reservoir by binding clay particles into flocculates.

Figure 9 shows that the dissolved and sand-sorbed components carry negligible amounts of cesium in the discharge water during flood conditions. This is because sand deposits quickly after entering the reservoir (Yamada et al., 2015). The relative contribution of dissolved cesium increases as the flood abates (Fig. 9). This tendency is consistent with the previous field studies (Nagao et al, 2013).

Table 2 shows the balance of sediment and ^{137}Cs migration within the Ogaki reservoir over the course of the simulation. It includes figures for reservoir inflow and outflow, deposition on the reservoir bed, and inventory remaining suspended within the reservoir water

245 after the end of the flood. All sand deposits on the reservoir bed. In contrast 3% of the silt and
246 75% of the clay flow downstream from the reservoir.

247 For ^{137}Cs, about 14% of the inflow is delivered via the reservoir outlet; 19% in the
248 silt-sorbed form, 73% in the clay-sorbed form and 7% in the dissolved form. These discharges
249 amounts are basically consistent with previous one and two-dimensional simulations of the
250 Ogaki Dam reservoir over the September 2013 flood (Kurikami et al., 2014; Yamada et al,
251 2015). The main reason for the slight difference is that this study considered
252 three-dimensional flows such as eddies, in addition to dispersion coefficients depending on
253 the dimension.

254 Figure S2 shows the profiles of horizontal flow velocities calculated at St. 1 and St. 2 as
255 a function of depth (vertical flow velocities were negligible). The profiles show that the inlet
256 water to the reservoir flows down on entering the reservoir to a water layer in the reservoir
257 with similar temperature (St.1). At monitoring station St.2, which lies further in the reservoir
258 from the inlet (Fig. 1), the flow velocities show a uniform profile with depth (Fig. S2). These
259 results are consistent with the monitoring data for October 2014 shown in Fig. S3. The
260 vertical profiles of concentration of suspended sediment were also qualitatively in good
261 agreement between the simulations and the monitoring results (Fig. S4 and Fig. S5).
262 Sediments concentrations are generally higher at St. 1 than at St. 2.

263 The above comparison between the Ogaki Dam simulation and the field results
264 demonstrate that the FLESCOT code gives realistic results when applied to a Fukushima
265 reservoir.

266

267 3.2 The effect of flood intensity on radiocesium discharge in generic model reservoirs

268

269 Forty-eight simulations were performed for generic model reservoirs to understand the

effect of reservoir volume, river inflow rate and flood duration on sediment and ^{137}Cs transport through the reservoirs. The proportions of discharge of sand, silt, clay and ^{137}Cs discharged from the reservoirs to the inflow over the generic floods are shown in Fig. 11(a), (b), (c) and (d). The proportions depend on the sediment grade, event intensity Q, event duration T and reservoir volume V.

Sand is the largest sediment grade in the simulations. Almost all the sand that enters a reservoir deposits on the bed, even when the total volume of water inflow is three times greater than the reservoir volume (QT/V=3.0 – Fig. 11(a)). Moderate sand discharges (up to 25% of the inflow) occur only for the largest reservoirs in the most intense events ($V \geq 1$ x10^7 m^3 and QT/V = 7.0).

Discharges of clay and silt increase significantly with the scale of the event (i.e. increasing QT/V – Fig. 11(b) and (c)). More than 65% of the clay inflow is discharged from the reservoir when QT/V=3.0 (Fig. 11(c)). At fixed QT/V, the discharge of clay shows relatively small variation with respect to different reservoir volumes V or lengths of the high inflow period T. For each reservoir volume, the discharge is higher when T is short (2.8 h) than when T = 28 h. This is because sediment particles are more likely to pass through the reservoir if there is limited time for deposition to occur.

By contrast silt shows a greater variation in discharge behavior at fixed QT/V than clay (Fig. 11(b)). Again discharge is higher in the shorter event periods (T = 2.8 h) than the longer events (T = 28 h) given the same total inflow QT and reservoir volume V. At fixed QT/V the discharge increases with the reservoir volume. This is because the dispersion coefficients assigned by equations (4) and (5) increase with the reservoir size.

The behavior of ^{137}Cs is strongly linked to transport of silt and clay (Fig. 11(d)). The discharge of ^{137}Cs increases from essential zero in the smallest flood events (QT/V = 0.3), to nearly complete discharge of the inflow at QT/V = 7.0 when the flood period is short (T =

295 2.8 h) or the reservoir is large (V=2.5x10^8 m^3)

296 Figure 12 shows the breakdown of how ^{137}Cs is discharged from the reservoirs, in terms
297 of the fraction of the discharge in sand, silt, clay-sorbed and dissolved forms. In low intensity
298 events (low QT/V or long T) discharged ^{137}Cs is mainly carried by clay (Fig. 12(c)). When
299 QT/V is large or T is short, the silt-sorbed form is the predominant transport mechanism
300 (Fig. 12(b)).

301 For comparison with the generic model reservoirs, the results of the Ogaki Dam reservoir
302 simulation over Typhoon Man-yi are shown on Figs. 11 and 12. The Ogaki reservoir volume
303 is V = 2.5x10^6 m^3. The Typhoon Man-yi event consisted of two spates of rainfall lasting 12 h
304 and 18 h over a 72 h period in September 2013. The total water inflow to the reservoir over
305 the event was QT = 6.5x10^6 m^3, giving QT/V = 2.6 for the event. The discharge proportions of
306 clay, silt, sand and ^{137}Cs are reasonably consistent with the results of the most comparable
307 model reservoir simulations (V = 1.0x10^6 m^3, QT/V = 2.0, 3.0). This shows the approximation
308 of the reservoir geometry introduced in the generic models (Fig. 6) does not have a large
309 bearing on the results.

310 Typhoon Etau in September 2015 was the largest flood to occur in Fukushima Prefecture
311 between March 2011 and May 2016. To gain an indication of the radiocesium discharge from
312 the Ogaki Dam reservoir over this event, we interpolated a discharge proportion from
313 Fig. 11(d). The event consisted of two peaks of rainfall within a 45 h period. The first rainfall
314 period lasted 3 h followed by a main rainfall period lasting 20 h. The total inflow was QT =
315 1.7x10^{7}m^3, giving QT/V = 6.8. It can be deduced fig. 11(d) that about 30% of radiocesium that
316 entered the Ogaki Dam reservoir during this typhoon flowed downstream to the lower Ukedo
317 River.

318

319 3.3 Effect of distribution coefficient on radiocesium discharge

The discharge of cesium from reservoirs depends on the distribution coefficients for absorption to sediments. In the limiting case of K_d = 0 m^3/kg, all ^{137}Cs remains dissolved and no deposition within the reservoir can occur. Therefore all the inflow is discharged downstream.

As K_d increases the opportunity for deposition grows, those lowering the proportion of discharge. The results of the simulations varying this parameter are shown in Fig. 13 (a). Figure 13 (b) shows the percentage of dissolved form in the total ^{137}Cs discharge, which also decreases as K_d increases.

In the case of the Ogaki Dam reservoir and other reservoirs in and around Fukushima, since the value of radiocesium distribution coefficient is large, radiocesium behavior is strongly affected by the behavior of suspended sediment (Fig. 13). On the other hand, in environments with high cation exchange capacity and low concentrations of mica-like minerals, low distribution coefficients lead to higher radiocesium discharges.

The catchments in Ukraine and Belarus affected by the Chernobyl accident are characterized by lower K_d values than Fukushima Prefecture (Evrard et al., 2015). Likewise the large releases of radiostrontium (^{89}Sr and ^{90}Sr) from the Chernobyl accident, which has a low distribution coefficient for absorption to sediments, differentiates the Chernobyl and Fukushima cases. The larger K_d values in Fukushima Prefecture means that countermeasures against sediment migration in reservoirs and water systems in Fukushima are likely to be more effective than would have been the case after the Chernobyl accident.

4. Conclusions

We performed a three-dimensional simulation of sediment and ^{137}Cs migration in the

345 Ogaki Dam reservoir in Fukushima Prefecture over Typhoon Man-yi. The simulation results
346 were consistent with various monitoring data, demonstrating the applicability of FLESCOT
347 for simulating Fukushima reservoirs.

348 We performed a study of generic model reservoirs to determine how radiocesium
349 discharges from reservoirs are affected by the reservoir volume, and flood parameters such as
350 inflow rate and flood duration. The analyses clarified the proportions of discharge of
351 sediments and ^{137}Cs out of a reservoir relative to the inflow under different conditions.

352 It is important to understand what kinds of sediment are the dominant carriers of the
353 ^{137}Cs during floods to effectively design countermeasures. If silt is dominant, silt fences may
354 be effective at reducing the outflow of radiocesium. If dissolved cesium is predominant,
355 sorbents such as zeolite can prevent radiocesium from entering areas of high importance, such
356 as paddy fields.

357 Our simulations did not consider the resuspension of contaminated bed sediment (we
358 assumed zero sediment and radiocesium in the reservoir the initial condition). Evrard et al.
359 (2014) suggested resuspension of contaminated bed sediment in typhoon and snow melt
360 seasons may not be negligible. Resuspension of bed sediment is more difficult to evaluate as
361 it requires measurements of the distribution of radioactivity in bed sediments to initialize
362 simulations. Still, our simulations show that reservoirs can accumulate radiocesium. This may
363 result in continuous contamination of fish in rivers and reservoirs in Fukushima Prefecture
364 (e.g. Nakata and Sugisaki, 2015).

365 From a scientific standpoint it is necessary to continue studies in Fukushima to quantify
366 the migration of contamination. Both field monitoring and simulations can contribute in this
367 respect. In particular, the results of the generic simulations reported here can be used to gauge
368 indicative values of discharges from reservoirs in Fukushima under different scales of flood
369 events. Such scoping results could then be used to target further studies, either through a field

monitoring program or bespoke simulation work, for sites with a high discharge risk.

Acknowledgments

The authors would like to thank the reviewers and editors for their comments and suggestions on the manuscript. We thank to the Tohoku Regional Agricultural Administration Office of MAFF for sharing the data. We appreciate Dr. Loren Eyler, Dr. Satoru T. Yokuda, Dr. Jie Bao and Dr. Kevin A. Glass of the Pacific Northwest National Laboratory, and Dr. Masahiko Machida, Dr. Mitsuhiro Itakura and Dr. Toshiyuki Nemoto of JAEA for improving the simulation code. We are grateful to Dr. Masahiko Okumura, Dr. Susumu Yamada for developing the grid of the reservoir and for discussions. We appreciate Dr. Toshiharu Misono and Mr. Kazuyuki Sakuma for managing the field data. We also thank Prof. Atsuyuki Suzuki of University of Tokyo, Mr. Yoshitake Shiratori and the members of Sector of Fukushima Research and Development of JAEA for supporting the study. The simulations were performed by the JAEA supercomputers, BX900 and ICE X.

References

Bulgakov, A.A., Konoplev, A.V., Smith, J.T., Hilton, J., Comans, R.N.J., Laptev, G.V., Christyuk, B.F., 2002. Modelling the long-term dynamics of radiocaesium in closed lakes. J. Environ. Radioact. 61, 41-53. DOI: 10.1016/S0265-931X(01)00113-8

Chartin, C., Evrard, O., Onda, Y., Patin, J., Lefevre, I., Ottle, C., Ayrault, S., Lepage, H., Bonte, P., 2013. Tracking the early dispersion of contaminated sediment along rivers draining the Fukushima radioactive pollution plume. Anthropocene, 1, 23-34. DOI:

10.1016/j.ancene.2013.07.001

Evrard, O., Chartin, C., Onda, Y., Patin, J., Lepage, H., Lefevre, I., Ayrault, S., Ottle, C., Bonte, P., 2013. Evolution of radioactive dose rates in fresh sediment deposits along coastal rivers draining Fukushima contamination plume. Sci. Rep. 3, 3079, DOI: 10.1038/srep03079.

Evrard, O., Chartin, C., Onda, Y., Lepage, H., Cerdan, O., Lefevre, I., Ayrault, S., 2014. Renewed soil erosion and remobilization of radioactive sediment in Fukushima coastal rivers after the 2013 typhoons. Sci. Rep. 4, 4574, DOI: 10.1038/srep04574.

Evrard, O., Laceby, J.P., Lepage, H., Onda, Y., Cerdan, O., Ayrault, S., 2015. Radiocesium transfer from hillslopes to the Pacific Ocean after the Fukushima Nuclear Power Plant accident: A review. J. Environ. Radioact. 148, 92-110. DOI: 10.1016/j.jenvrad.2015.06.018.

IAEA, 2001. Generic models for use in assessing the impact of discharges of radioactive substances to the environment, Safety Reports Series No. 19, Vienna.

IAEA, 2006. Environmental consequences of the Chernobyl accident and their remediation: twenty years of experience, Report of the Chernobyl Forum Expert Group 'Environment', Radiological assessment reports series, STI/PUB/1239, Vienna.

Japan Atomic Energy Agency, 2013a. Investigation and Study of the Secondary Distribution of Radioactive Substances due to the Accident at the Fukushima Daiichi Nuclear Power Plant, (accessed 05.12.16.) at http://www.jaea.go.jp/fukushima/kankyoanzen/mapping_report/2nd-japanese/2ndlist.html (in Japanese).

Japan Atomic Energy Agency, 2013b. Establishment of Technique for Identifying Long-term Impact of Radioactive Substances due to the Accident at the Fukushima Dai-ichi Nuclear Power Plant, (accessed 05.12.16) at

http://fukushima.jaea.go.jp/initiatives/cat03/entry05.html (in Japanese).

Japan Dam Foundation, 2015. Dams in Japan 2015, http://damnet.or.jp/Dambinran/binran/TopIndex.html, accessed November 16, 2015.

Kurikami, H., Kitamura, A., Yokuda, S.T., Onishi, Y., 2014. Sediment and ^{137}Cs behaviors in the Ogaki Dam Reservoir during a heavy rainfall event. J. Environ. Radioact. 137, 10-17. DOI: 10.1016/j.jenvrad.2014.06.013

Ministry of Agriculture, Forestry and Fisheries, 2014. Results of radiocesium investigation in the Ogaki Dam reservoir (accessed 06.24.16) at http://www.maff.go.jp/tohoku/osirase/higai_taisaku/hukkou/140918_torimatome.html (in Japanese).

Ministry of Economy, Trade and Industry, 2013. Restricted areas and areas to which evacuation orders have been issued (March 7, 2013). (accessed 05.30.16) at http://www.meti.go.jp/english/earthquake/nuclear/roadmap/pdf/20130307_01.pdf

Mouri, G., Golosov, V., Shiiba, M., Hori, T., 2014. Assessment of the caesium-137 flux adsorbed to suspended sediment in a reservoir in the contaminated Fukushima region in Japan. Environ. Pollut. 187, 31-41. DOI: 10.1016/j.envpol.2013.12.018

Nagao, S., Kanamori, M., Ochiai, S., Tomihara, S., Fukushi, K., Yamamoto, M., 2013. Export of ^{134}Cs and ^{137}Cs in the Fukushima river systems at heavy rains by Typhoon Roke in September 2011. Biogeosciences 10, 6215-6223.

Nakata, K., Sugisaki, H. (eds.), 2015. Impacts of the Fukushima Nuclear Accident of Fish and Fishing Grounds. Springer Open. DOI: 10.1007/978-4-431-55537-7

National Spatial Planning and Regional Policy Bureau (Ministry of Land, Infrastructure, Transport and Tourism), 2016. Natural Land Numerical Information (accessed 06.20.16.) at http://nlftp.mlit.go.jp/ksj-e/

Nishimura, H., Touch, N., Komai, K., Hibino, T., 2009. Modeling of Settling Velocity

445 Considering Organic Property of Suspended Organic Matter. J. Jpn. Soc. Civ. Eng., Ser.
446 B2. 65, 1151-1155. DOI: 10.2208/kaigan.65.1151 (in Japanese with English abstract)
447 Nuclear Regulation Authority, 2016. Monitoring information of environmental radioactivity
448 level (accessed 06.20.16.) at http://radioactivity.nsr.go.jp/en/
449 Ochiai, S., Nagao, S., Yamamoto, M., Itono, T., Kashiwaya, K., Fukui, K., Iida, H., 2013.
450 Deposition records in lake sediments in western Japan of radioactive Cs from the
451 Fukushima Dai-ichi nuclear power plant accident. Appl. Radiat. Isot. 81, 366-370. DOI:
452 10.1016/j.apradiso.2013.03.073
453 Onishi, Y., Trent, D.S., 1985. Three-Dimensional Simulation of Flow, Salinity, Sediment, and
454 Radionuclides Movements in the Hudson River Estuary. In Proceedings of the 1985
455 Specialty Conference of the Hydraulic Division, pp. 1095−1100, American Society of
456 Civil Engineers, August 12-17, 1985, Lake Buena Vista, Florida.
457 Onishi, Y., 1987. A Three-Dimensional Flow, Energy, Salinity, Sediment and Contaminant
458 Transport (FLESCOT) Model for Ocean Disposal of Low-Level Radioactive Waste. In
459 Proceedings of the Workshop on Ocean Modeling Efforts at EPA, pp. 37−49, February
460 10, 1987, Washington, D. C.
461 Onishi, Y., Trent, D.S., 1992. Turbulence Modeling for Deep Ocean Radionuclide. Int. J,
462 Numer. Methods Fluids 15, 1059-1071. DOI: 10.1002/fld.1650150910
463 Onishi, Y., Graber, H.C., Trent, D.S., 1993. Preliminary Modeling of Wave-enhanced
464 Sediment and Contaminant Transport in New Bedford Harbor, Coastal and Estuarine
465 Studies, Vol. 42, Nearshore and Estuarine Cohesive Sediment Transport, A. J. Mehta ed.,
466 American Geophysical Union. DOI: 10.1029/CE042p0541
467 Otsubo, K., 1983. Experimental Studies on the Physical Properties of Mud and the
468 Characteristics of Mud Transportation, Research Report from the National Institute for
469 Environmental Studies, Japan, No. 42. (in Japanese with English abstract)

Smith, J.T., Konoplev, A., Bulgakov, A.A., Comans, R.N.J., Cross, M.A., Kaminski, S., Khristuk, B., Klemt, E., de Koning, A., Kudelsky, A.V., Laptev, G., Madruga, M.J., Voitsekhovitch, O., Zibold, G., 2002. AQUASCOPE Technical Deliverable. Simplified models for predicting ^{89}Sr, ^{90}Sr, ^{134}Cs, ^{137}Cs, ^{131}I in water and fish of rivers, lakes and reservoirs, CEH Centre for Ecology and Hydrology, Natural Environment Research Council.

Spezzano, P., Hilton, J., Lishman, J.P., Carrick, T.R., 1993. The variability of Chernobyl Cs retention in the water column of lakes in the English Lake District, two years and four years after deposition. J. Environ. Radioact. 19, 213-232. DOI: 10.1016/0265-931X(93)90004-Q

Teeter, A.M., 1988. New Bedford Harbor Superfund Project, Acushnet River Estuary Engineering Feasibility Study of Dredging and Dredged Material Disposal Alternatives, Report 2 Sediment and Contaminant Hydraulic Transport Investigations. Technical Report EL-88-15. U.S. Army Corps of Engineers, Vicksburg, Mississippi.

Ueda, S., Hasegawa, H., Kakiuchi, H., Akata, N., Ohtsuka, Y., Hisamatsu, S., 2013. Fluvial discharges of radiocaesium from watersheds contaminated by the Fukushima Dai-ichi Nuclear Power Plant accident, Japan. J. Environ. Radioact. 118, 96-104. DOI: 10.1016/j.jenvrad.2012.11.009

United States Environmental Protection Agency, 1999. Understanding variation in partition coefficient, Kd, values, Volume II: review of geochemistry and available Kd values for cadmium, cesium, chromium, lead, plutonium, radon, strontium, thorium, tritium (3H), and uranium, EPA 402-R-99-004B.

Vanoni, V.A. (Ed.), 1975. Sedimentation Engineering, ASCE Manuals and Report on Engineering Practice. American Society of Civil Engineers, New York.

Yamada, S., Kitamura, A., Kurikami, H., Yamaguchi, M., Malins, A., Machida, M., 2015.

Sediment and ^{137}Cs transport and accumulation in the Ogaki Dam of eastern Fukushima. Environ. Res. Lett. 10, 014013. DOI: 10.1088/1748-9326/10/1/014013

Yamashiki, Y., Onda, Y., Smith, H.G., Blake, W.H., Wakahara, T., Igarashi, Y., Matsuura, Y., Yoshimura, K., 2014. Initial flux of sediment-associated radiocesium to the ocean from the largest river impacted by Fukushima Daiichi Nuclear Power Plant. Sci. Rep. 4, 3714. DOI:10.1038/srep03714

Figure captions

Figure 1 The location of the Ogaki Dam reservoir, the Fukushima Dai-ichi NPP and the location of monitoring stations. Shading shows ^{137}Cs fallout deposition densities. The dam is located in a heavily contaminated area. River discharge rates, concentrations of suspended sediment and radiocesium were monitored at stations upstream and downstream of the reservoir. Depth profiles of flow velocity, turbidity and temperature are monitored at the stations St.1 and St.2. The deposition densities are from Nuclear Regulation Authority website (2016). Topography and river data are from the National Land Numerical Information © 1974-2013 National Information Division, National Spatial Planning and Regional Policy Bureau, MLT of Japan.

Figure 2 Topography of the bed of the Ogaki Dam reservoir. The average reservoir water depth is 9.1 m when the water height is set at 140 m above sea level.

Figure 3 The discharge rates at the inflow to the Ogaki reservoir. These data were applied as the boundary condition for the simulation of the Ogaki Dam over September 2013 Typhoon Man-yi. The measured values shown are the sum of data from the Hirusone and the Yaguno stations.

Figure 4 The concentration of suspended sediment applied as the inflow boundary condition. The values from September 16, 6:00 to September 17, 12:00 were estimated from the relationship between river discharge rates and sediment concentrations at other times.

Figure 5 The concentration of ^{137}Cs applied as the inflow boundary condition. The concentrations of particulate and dissolved cesium were estimated from the total cesium concentration and the distribution coefficients of sand, silt and clay.

Figure 6 The model used for the sensitivity analysis. The number of computational cells is 10,000 (10x100x10). The cell sizes in the longitudinal, transverse and vertical directions are $a/10$, $a/10$ and $a/100$, respectively, where a is the total width of the reservoir.

Figure 7 The river inflow rate employed in the sensitivity analyses.

Figure 8 Comparison between measured and simulated concentrations of suspended sediment at the outlet of the Ogaki Dam reservoir over 2013 Typhoon Man-yi.

Figure 9 Comparison between the measured and simulated concentration of ^{137}Cs at the outlet of the Ogaki Dam reservoir over Typhoon Man-yi.

Figure 10 Suspended sediment particles within water taken from the inlet and outlet of the Ogaki Dam reservoir, as seen through a microscope.

Figure 11 The proportions of discharge of (a) sand, (b) silt, (c) clay and (d) ^{137}Cs discharged from the model reservoirs as a percentage of the inflow over the generic floods.

Figure 12 Breakdown of the ^{137}Cs discharge. Proportions of the total ^{137}Cs discharge in the (a) sand-sorbed, (b) silt-sorbed, (c) clay-sorbed and (d) dissolved forms over the model floods.

Figure 13 Effect of the distribution coefficient on (a) the proportion of ^{137}Cs. discharge to the total inflow and (b) the proportion of dissolved ^{137}Cs in the discharge. The sand:silt:clay distribution coefficient ratio is fixed as 3:50:50 in the simulations.

Figure 1

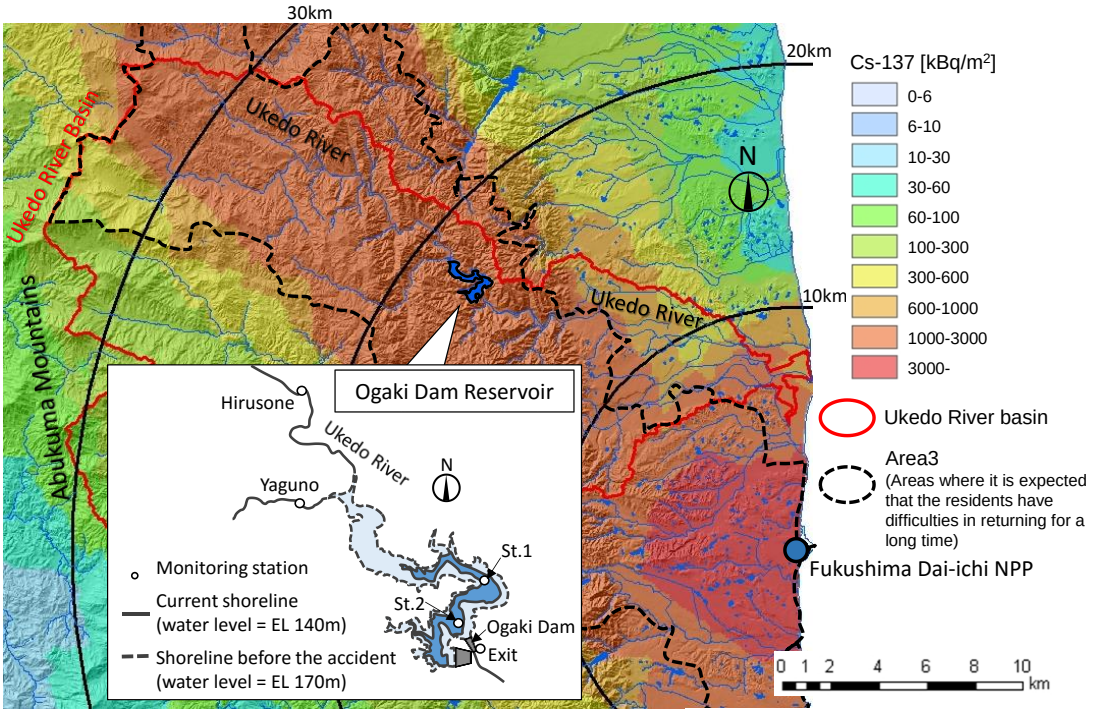

Figure 2

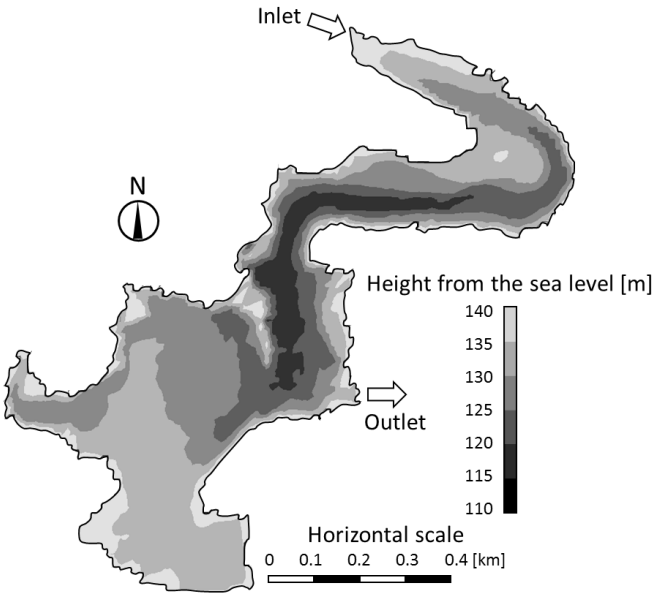

Figure 3

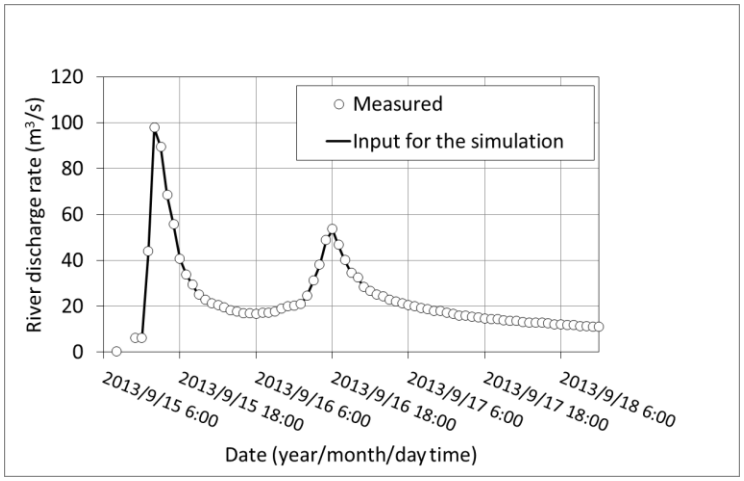

Figure 4

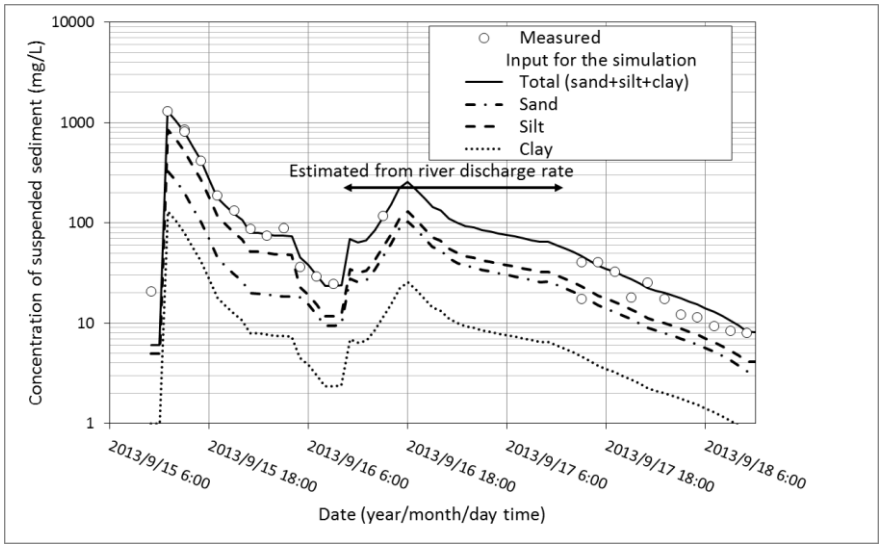

Figure 5

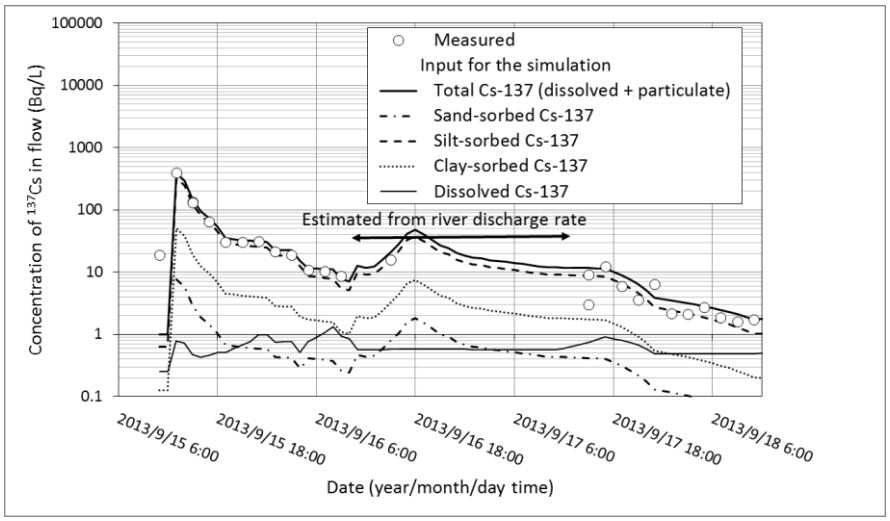

Figure 6

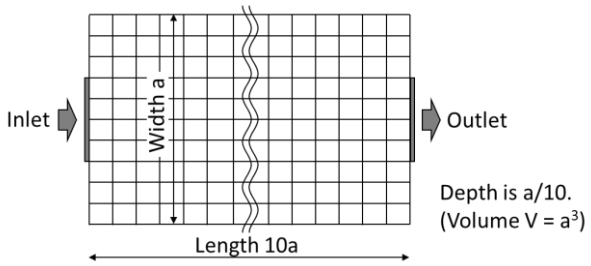

Figure 7

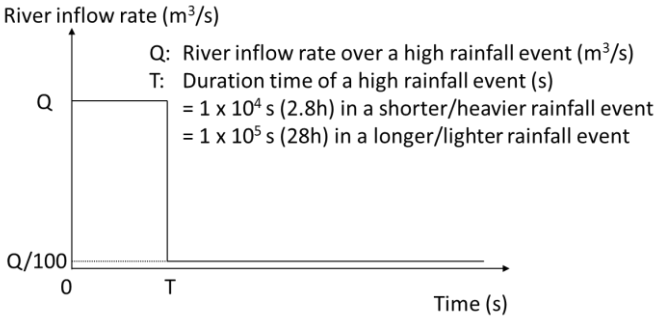

Figure 8

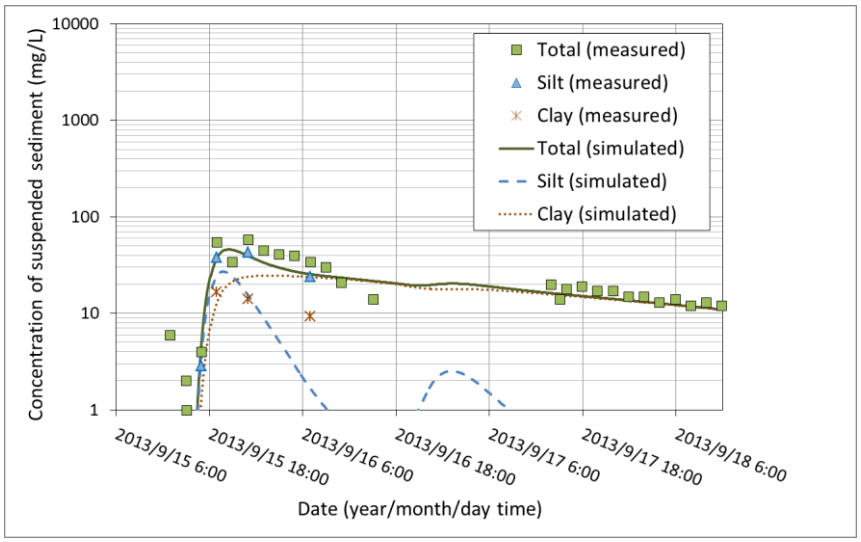

Figure 9

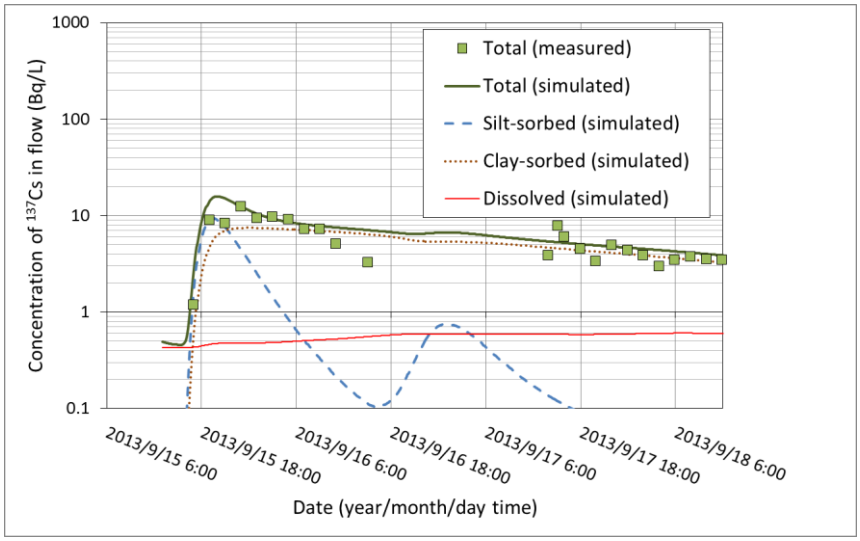

Figure 10

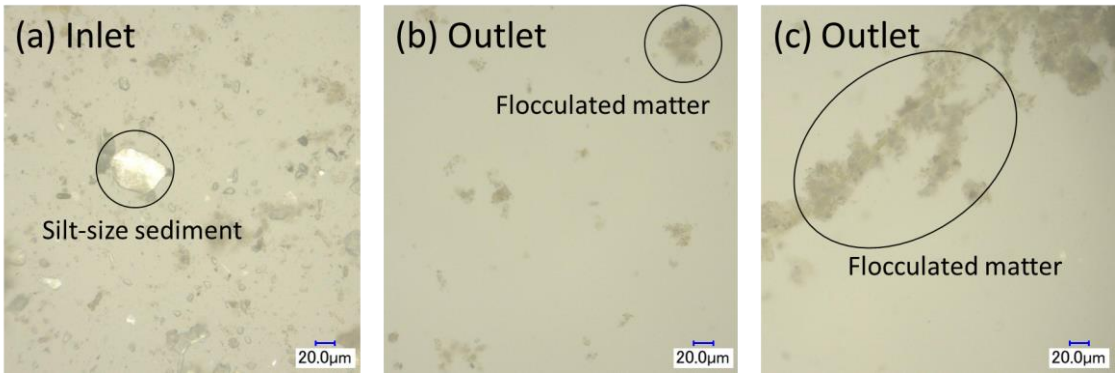

Figure 11

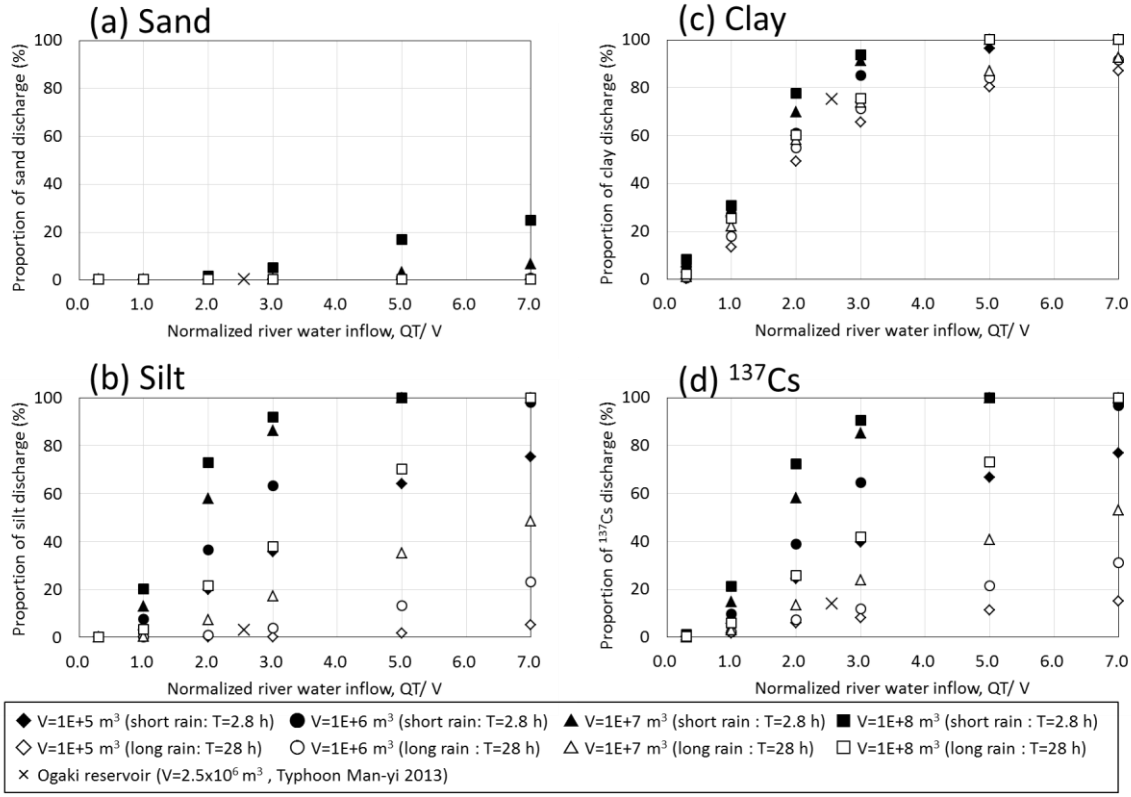
(a) Sand
Proportion of sand discharge (%)
Normalized river water inflow, QT/ V
(c) Clay
Proportion of clay discharge (%)
Normalized river water inflow, QT/ V
(b) Silt
Proportion of silt discharge (%)
Normalized river water inflow, QT/ V
(d) 137Cs
Proportion of 137Cs discharge (%)
Normalized river water inflow, QT/ V
V=1E+5 m3 (short rain: T=2.8 h)
V=1E+6 m3 (short rain: T=2.8 h)
V=1E+7 m3 (short rain : T=2.8 h)
V=1E+8 m3 (short rain : T=2.8 h)
V=1E+5 m3 (long rain: T=28 h)
V=1E+6 m3 (long rain : T=28 h)
V=1E+7 m3 (long rain : T=28 h)
V=1E+8 m3 (long rain : T=28 h)
Ogaki reservoir (V=2.5x10^6 m3 , Typhoon Man-yi 2013)

Figure 12

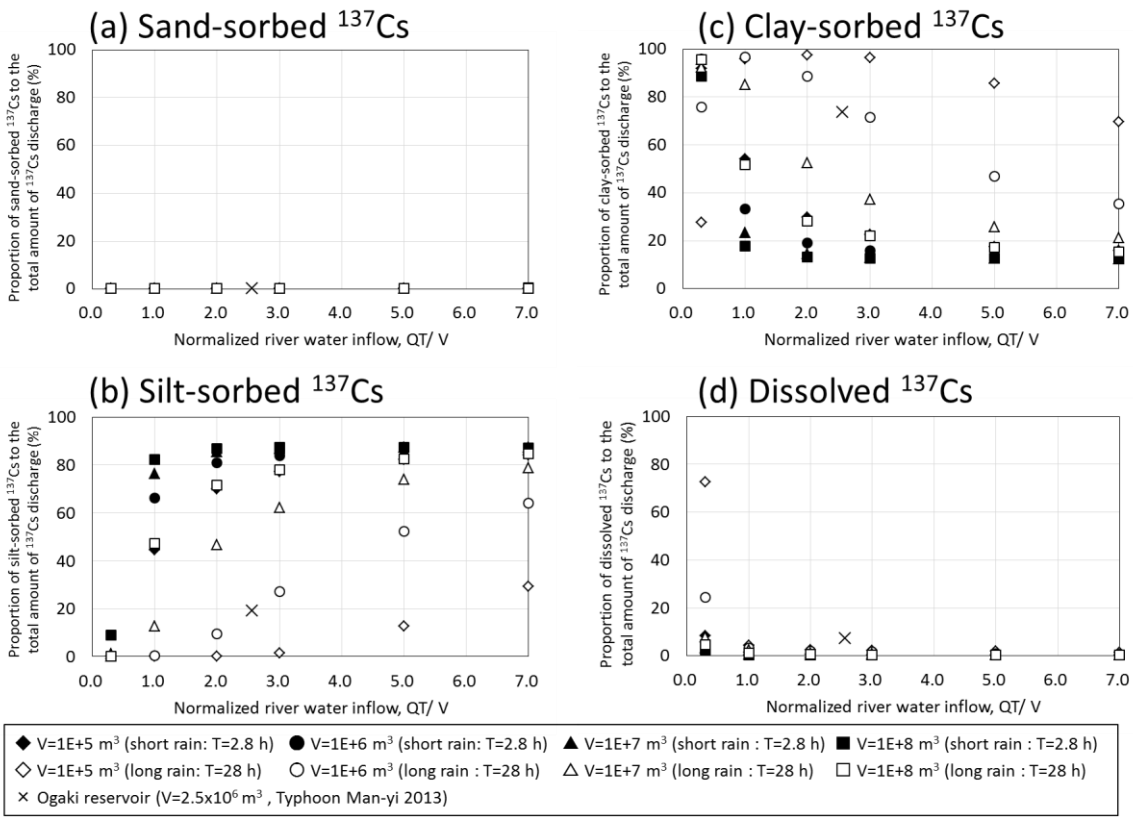
(a) Sand-sorbed 137Cs
Proportion of sand-sorbed 137Cs to the total amount of 137Cs discharge (%)
Normalized river water inflow, QT/ V
(c) Clay-sorbed 137Cs
Proportion of clay-sorbed 137Cs to the total amount of 137Cs discharge (%)
Normalized river water inflow, QT/ V
(b) Silt-sorbed 137Cs
Proportion of silt-sorbed 137Cs to the total amount of 137Cs discharge (%)
Normalized river water inflow, QT/ V
(d) Dissolved 137Cs
Proportion of dissolved 137Cs to the total amount of 137Cs discharge (%)
Normalized river water inflow, QT/ V
◆ V=1E+5 m3 (short rain: T=2.8 h)
● V=1E+6 m3 (short rain: T=2.8 h)
▲ V=1E+7 m3 (short rain : T=2.8 h)
■ V=1E+8 m3 (short rain : T=2.8 h)
◇ V=1E+5 m3 (long rain: T=28 h)
○ V=1E+6 m3 (long rain : T=28 h)
△ V=1E+7 m3 (long rain : T=28 h)
□ V=1E+8 m3 (long rain : T=28 h)
× Ogaki reservoir (V=2.5x10^6 m3 , Typhoon Man-yi 2013)

Figure 13

(a)

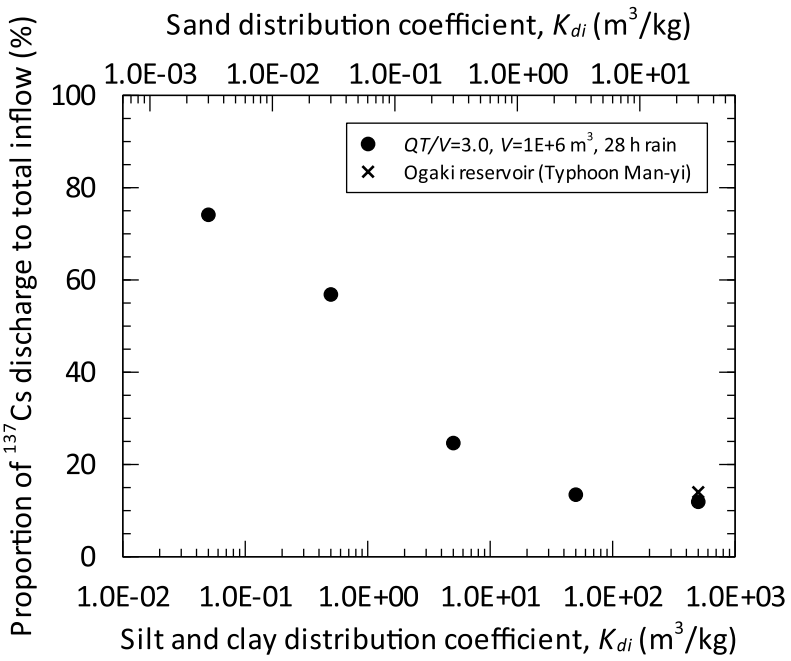
Sand distribution coefficient, K_{di} (m^3/kg)
1.0E-03
1.0E-02
1.0E-01
1.0E+00
1.0E+01
100
80
60
40
20
0
Proportion of ^{137}Cs discharge to total inflow (%)
QT/V=3.0, V=1E+6 m^3, 28 h rain
Ogaki reservoir (Typhoon Man-yi)
1.0E-02
1.0E-01
1.0E+00
1.0E+01
1.0E+02
1.0E+03
Silt and clay distribution coefficient, K_{di} (m^3/kg)

(b)

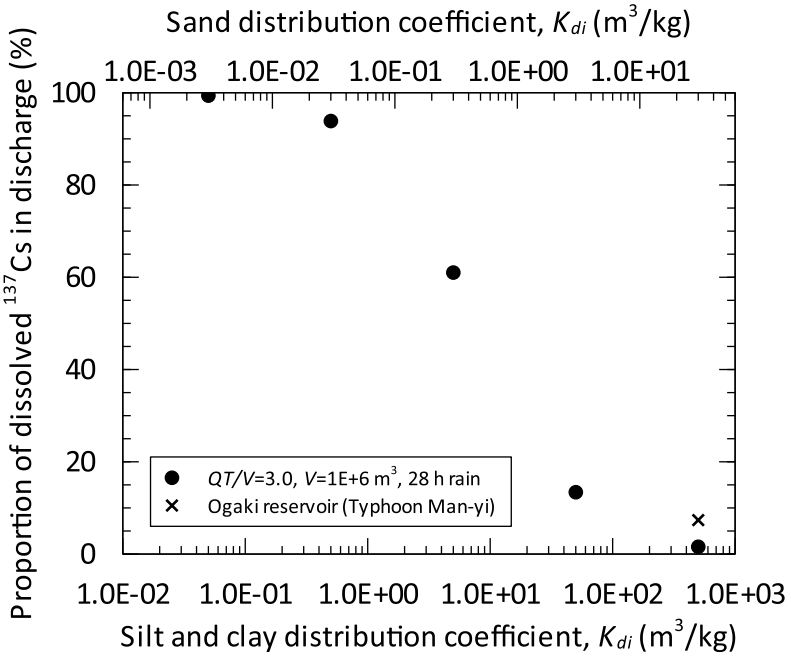
Sand distribution coefficient, K_{di} (m^3/kg)
1.0E-03
1.0E-02
1.0E-01
1.0E+00
1.0E+01
100
80
60
40
20
0
Proportion of dissolved ^{137}Cs in discharge (%)
QT/V=3.0, V=1E+6 m^3, 28 h rain
Ogaki reservoir (Typhoon Man-yi)
1.0E-02
1.0E-01
1.0E+00
1.0E+01
1.0E+02
1.0E+03
Silt and clay distribution coefficient, K_{di} (m^3/kg)

Table captions

Table 1 The parameters used in the simulation of the Ogaki Dam reservoir for Typhoon Man-yi (September 2013).

Table 2 The balance of sediment and ^{137}Cs migration across the Ogaki Dam reservoir over the course of 2013 Typhoon Man-yi (simulation results).

Table 1

Parameter	Value	Reference
Representative particle sizes	Sand: 2.8E-3 m Silt: 3.6E-5 m Clay: 4.2E-6 m	Estimated from field samples (taken at the Hirusone station) (MAFF, private communication, January 28, 2014)
Sand transport model	Du Boys	Vanoni (1975)
Critical shear stress for deposition	Silt: 0.05 Pa Clay: 0.01 Pa	Estimated from literature (Onishi et al., 1993; Otsubo, 1983)
Erodibility	4E-6 $kg/m^2/s$	Teeter (1988)
Dispersion coefficient	Horizontal: 5 m^2/s Vertical: 0.01 m^2/s	Estimated Eqs. (4) and (5) (IAEA, 2001)
Distribution coefficient	Sand: 30 m^3/kg Silt: 500 m^3/kg Clay: 500 m^3/kg	Based on results from field samples (JAEA, 2013a, 2013b)
Mass transfer rate for dissolved contaminant adsorption to and desorption from suspended sediment	5E-8 s^{-1}	Assumed
Mass transfer rate for dissolved contaminant adsorption to and desorption from bed sediment	5E-11 s^{-1}	Assumed
Settling velocity	Sand: 7.0E-2 m/s Silt: 1.2E-3 m/s Clay: 1.6E-5 m/s	Estimated from Stokes' law

Table 2

	Sand (kg)	Silt (kg)	Clay (kg)	^{137}Cs (Bq)
Total inflow to the reservoir	4.3E+5	9.3E+5	1.5E+5	3.4E+11
Deposited onto the bed	4.3E+5 (100%)	9.0E+5 (97%)	3.1E+4 (21%)	2.9E+11 (85%)
Suspended in the reservoir	0 (0%)	0 (0%)	6.7E+3 (4%)	3.0E+9 (1%)
Discharged from the reservoir	0 (0%)	2.7E+4 (3%)	1.1E+5 (75%)	4.7E+10 (14%) 19% in silt-sorbed form, 73% clay-sorbed, 7% dissolved

Supplementary Information: Figure captions

Figure S1 The temperature profile of the reservoir water with depth at the St. 1 and St. 2 monitoring stations, Ogaki Dam reservoir. The solid line is a discretization of the measurement data used as a simulation input.

Figure S2 Simulation results: horizontal flow velocities as a function of depth at St.1 and St.2.

Figure S3 Monitoring results: horizontal flow velocities as a function of depth at St.1 and St.2. Note the monitoring period is different from the simulation period. However the simulated flow velocities are within the range of the monitoring results.

Figure S4 Simulation results: vertical distribution of suspended sediment concentrations at St.1 and St.2.

Figure S5 Monitoring results: vertical distribution of turbidity at St.1 and St.2.

Figure S1

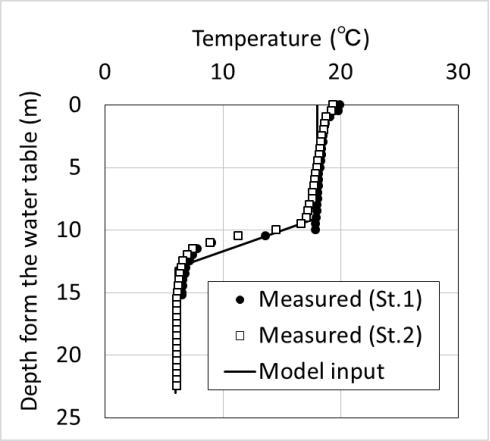
Temperature (℃)
0
10
20
30
Depth form the water table (m)
0
5
10
15
20
25
Measured (St.1)
Measured (St.2)
Model input

Figure S2

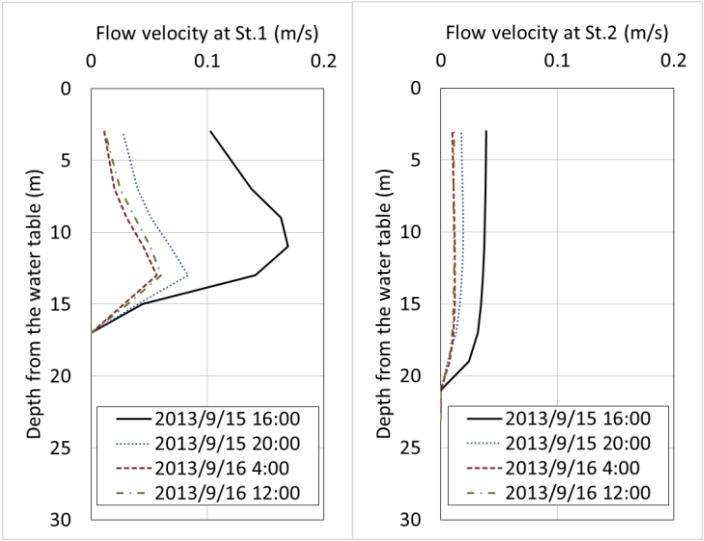

Figure S3

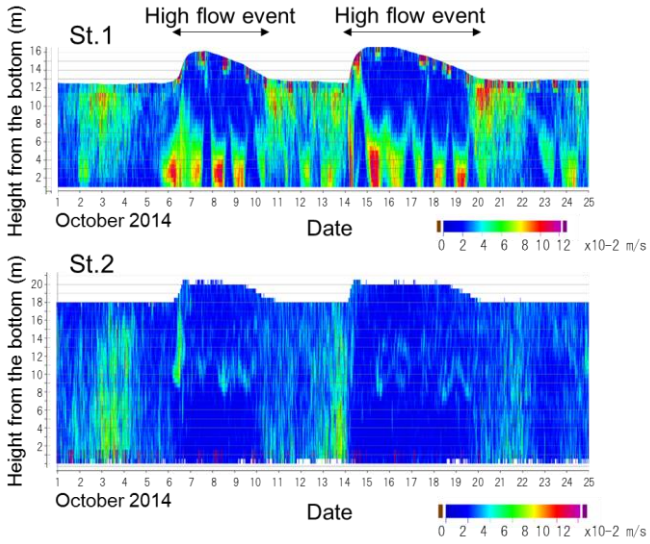

Figure S4

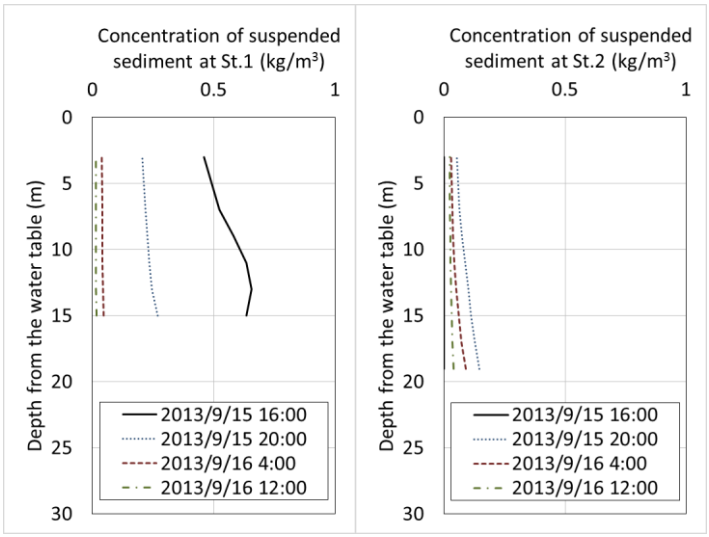

Figure S5